ACS Partner Journal
CHEM & BIO ENGINEERING

Open Access
This article is licensed under CC-BY-NC-ND 4.0

pubs.acs.org/ChemBioEng
Article

# Ni−Fe Nanoparticles Supported on UiO-66-X Catalyst for Hydrogenation of Fatty Acid Esters to Alcohols

Pengcheng Li, Tianyu Ma, Youyang Wu, Jianping Wu, Haoran Yu, Lirong Yang, and Gang Xu*

Cite This: *Chem Bio Eng.* 2025, 2, 23−34
Read Online

ACCESS | Metrics & More | Article Recommendations | Supporting Information

**ABSTRACT:** Enhancing the performance of non-noble-metal catalysts would facilitate the economic feasibility of the chemical conversion process. Through strategies involving metal nanoparticles (MNPs) size control and support functionalization modification, Ni2Fe6/UiO-66-X-y catalysts (X stands for H, OH, $CH_3$, and $NH_2$, and y stands for the concentration of $NaBH_4$ solution) were prepared for the efficiently selective hydrogenation of methyl laurate (ML) to 1-dodecanol. High-concentration $NaBH_4$ solution facilitated the preparation of smaller-sized MNPs, while support functionalization could alter the chemical microenvironment of the support, thereby promoting electron transfer between appropriately sized MNPs and the support. In particular, the Ni2Fe6/UiO-66-$NH_2$-0.4 M catalyst could achieve 99.9% conversion of ML and 98.6% selectivity for 1-dodecanol when it was reacted at 220 °C and 3 MPa $H_2$ for 8 h. The probable catalytic mechanism based on the $\eta^2$(C, O)-aldehyde conformation was discussed, and reaction kinetics were calculated. Furthermore, the catalyst achieved five stable recycling runs and demonstrated catalytic versatility for other fatty acid methyl esters, including methyl stearate, methyl palmitate, and methyl valerate.

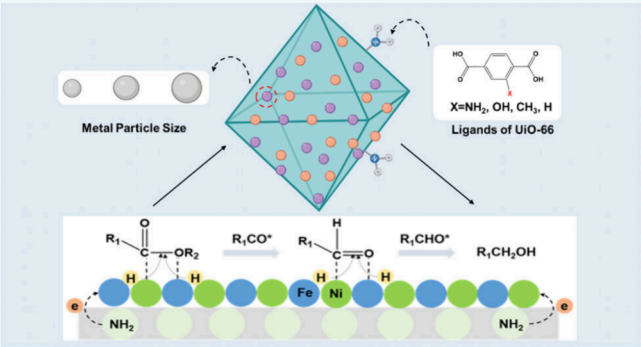


**KEYWORDS:** *UiO-66-X, Ni−Fe nanoparticles, hydrogenation, fatty acid methyl esters, fatty alcohol*

## 1. INTRODUCTION

Natural fats are composed of triglycerides and free fatty acids, which are widely found in plant oils and animal fats.[1] Fatty alcohols represent value-added products derived from the chemical conversion of fatty acid methyl esters via selective hydrogenation, finding widespread applications in pharmaceuticals, fragrances, and emulsifiers.[2−4] However, the inherently low reactivity of the carbonyl group in carboxylic acid esters necessitates a strong reliance on catalyst performance for this type of reaction.[2,5] Noble metals like Pd and Ru display excellent catalytic activity but are economically prohibitive for large-scale applications.[6,7] The activity and stability of common metal catalysts can be significantly enhanced through metal−support interactions, involving the tuning of composition, particle size of MNPs, and support properties.[8,9]

Common transition metals have been the focus of much research in heterogeneous hydrogenation of fatty acid methyl esters.[10] Unfortunately, common metals such as Ni, Fe, and Zn yield low fatty alcohol production when used individually, leading to their combination in hydrotransformation processes to achieve synergistic effects.[11,12] Notably, Ni and Co have low oxophilicity and tend to bind to carbon atoms of the ester group via $\eta^1$(C)-acyl adsorption configuration, leading to decarbonylation/decarboxylation (DCN/DCX) reactions and resulting in the production of alkanes with one fewer carbon chain.[5,10,13,14] Conversely, Fe tends to bind to oxygen atoms due to its moderate oxophilicity, doping it into Ni undergoes direct hydrodeoxygenation (HDO) via $\eta^2$(C, O)-aldehyde conformation to obtain fatty alcohols.[12,15,16]

The electron transfer between MNPs and the support at the Fermi energy level is influenced by the size of the MNPs.[17] Studies on the modulation of metal−support interaction typically involve MNPs smaller than 5 nm.[8] For instance, Wang et al.[18] reported that in Pd-catalyzed reactions, the selectivity exhibited volcano trend dependence on particle size, with geometrical and electronic effects dominating the reaction at larger (>4 nm) and smaller (<4 nm) sizes, respectively. Furthermore, the reduction of particle size results in higher surface free energy and a larger specific surface area, consequently lowering reaction barriers and enhancing catalyst utilization in the reaction.[19] Tuning the metal−support interaction can also be accomplished by introducing functional

**Received:** May 26, 2024
**Revised:** September 4, 2024
**Accepted:** September 6, 2024
**Published:** September 16, 2024

ACS Publications
© 2024 The Authors. Co-published by Zhejiang University and American Chemical Society

groups to modify the surface of the support. Specific functional groups can be tailored according to the chemical microenvironment required for the reaction and MNPs, thereby altering the electron structure of the metal.[8,20,21] Moreover, small-sized MNPs with a high surface energy are susceptible to agglomeration. Immobilizing them onto support with high specific surface area and easy modification represents an effective approach for enhancing catalytic performance.[22,23]

A distinctive advantage of metal−organic frameworks (MOFs) over conventional supports lies in their capacity to modify various functionalized groups within the structure through in situ synthesis or postmodification methods. This capability grants MOFs a unique chemical microenvironment.[24−26] UiO-66, featuring Zr(IV) as the metal node and terephthalic acid ($H_2BDC$) as the organic ligand, demonstrates excellent thermal stability and high specific surface area.[27,28] Of significance, functionalized derivatives of $H_2BDC$ ($H_2BDC$-X) can replace $H_2BDC$, resulting in the surface chemically modified material UiO-66-X.[29] This capability proves highly beneficial in adjusting the chemical microenvironment of MNPs on the support.[30,31] UiO-66 and its derivative materials have served as excellent supports for heterogeneous hydrogenation.[32−34]

Building upon prior research,[35] the activity of the Ni2Fe6/UiO-66 catalyst was optimized through strategies involving particle size control and regulation of the chemical microenvironment of the support. This optimization facilitated the efficient and selective hydrogenation of fatty acid methyl esters. It was demonstrated that the optimal catalytic combination Ni2Fe6/UiO-66-$NH_2$-0.4 M could achieve an ML conversion of 99.9% and 1-dodecanol selectivity of 98.6% when reacted at 220 °C and 3 MPa $H_2$ for 8 h. The conformational relationships of the catalysts were analyzed using multiple characterization techniques, and the reaction mechanisms were discussed. Additionally, the recycling stability and versatility of the catalysts were investigated.

## 2. EXPERIMENTAL SECTION

**2.1. Chemicals.** Terephthalic acid (A.R.), nickel acetate (A.R.), methyl palmitate (A.R.), methyl stearate (A.R.), methyl valerate (A.R.) and 1-pentanol (A.R.) were purchased from Aladdin Bio-Chem Technology Co., Ltd. (Shanghai, China). Zirconium chloride (A.R.), 2-aminoterephthalic acid (A.R.), 2-hydroxyterephthalic acid (A.R.), lauroic acid (A.R.), n-undecane (A.R.), n-dodecane (A.R.), ferrous sulfate heptahydrate (A.R.), methyl laurate (A.R.), 1-dodecanol (A.R.), n-hexadecane (A.R.) were purchased from Macklin Biochemical Co., Ltd. (Shanghai, China). Polyvinylpyrrolidone K30 (G.R.), N,N-dimethylformamisde (A.R.), acetic acid (A.R.), sodium borohydride (98%), acetone (A.R.), 1,4-dioxane (A.R.), ethanol (A.R.) and methanol (A.R.) were purchased from Sinopharm Chemical Reagent Co., Ltd. (Shanghai, China). 1-Hexadecanol (A.R.) purchased from Rhawn Chemical Technologies Ltd. (Shanghai, China). 2-Methyl-1,4-benzenedicarboxylic acid (A.R.) purchased from Shanghai Mayer Biochemical Technology Co., Ltd. 1-Octadecanol was purchased from Bide Pharmatech Ltd. (Shanghai, China). Hydrogen (>99.99%), nitrogen (>99.99%) and air (>99.99%) were obtained from Hangzhou Minxing Chemical Technology Co., Ltd. All reagents were used directly in the next processes without further purification.

**2.2. Preparation of Ni2Fe6/UiO-66-X-y Catalysts.** The preparation of Ni2Fe6/UiO-66-X-y catalysts (X stands for H, OH, $CH_3$, $NH_2$, and y stands for the concentration of $NaBH_4$ solution) involved two steps: the preparation of UiO-66-X and the loading of Ni−Fe MNPs.

*Preparation of UiO-66-X.* As example, UiO-66-$NH_2$ was prepared by a solvothermal method with modifications based on previous reports.[31] In a round-bottomed flask, anhydrous zirconium chloride ($ZrCl_4$, 300.0 mg, 1.29 mmol), 2-aminoterephthalic acid (217.4 mg, 1.20 mmol), and acetic acid (4 mL) were dissolved in 30 mL of N,N-dimethylformamide (DMF) and ultrasonicated for 30 min. The mixture was then transferred to an autoclave lined with polytetrafluoroethylene, sealed, placed in a preheated oven, and heated to crystallize at 130 °C for 12 h. After the mixture was cooled to room temperature, the crystals formed were collected by centrifugation at 8000 rpm for 10 min. The solid obtained by centrifugation was washed by DMF to remove the residual precursor, and then solvent exchanged by methanol to remove the DMF. Finally, the solid was dried under vacuum at 60 °C for 4 h, and then dried in an oven at 80 °C overnight to obtain UiO-66-$NH_2$ powder. UiO-66-H (UiO-66), UiO-66-$CH_3$, and UiO-66-OH were prepared similarly to UiO-66-$NH_2$, utilizing $ZrCl_4$ (300.0 mg, 1.29 mmol) as the metal precursor and terephthalic acid (200.0 mg, 1.20 mmol), 2-methylterephthalic acid (216.2 mg, 1.20 mmol), and 2-hydroxyterephthalic acid (218.6 mg, 1.20 mmol) as the organic ligands. For convenience, UiO-66-H, UiO-66-$NH_2$, UiO-66-$CH_3$, and UiO-66-OH are collectively referred to as UiO-66-X (X stands for H, $NH_2$, $CH_3$, OH).

*Preparation of Ni2Fe6/UiO-66-X-y Catalysts.* Ni2Fe6/UiO-66-X-y catalysts were prepared by a liquid-phase impregnation reduction method. In a typical preparation process, Ni2Fe6/UiO-66-$NH_2$-0.4 M catalysts with a theoretical metal loading of 10 wt % were synthesized as follows: 453 mg of UiO-66-$NH_2$ and 200 mg of polyvinylpyrrolidone (PVP) K30 were dispersed in 20 mL of deionized water containing 0.2 mmol of $Ni(CH_3COO)_2{\cdot}4H_2O$ and 0.6 mmol of $FeSO_4{\cdot}7H_2O$. The mixture was sonicated for 30 min and stirred for 4 h. In an ice−water bath, 10 mL of 0.4 M $NaBH_4$ solution was slowly added dropwise to the mixture to reduce the metal ions. Subsequently, the solution changed color to black, indicating the formation of MNPs. The mixture was stirred continuously for 30 min and then left to age overnight. Finally, the solid was centrifuged at 8000 rpm for 10 min after the addition of acetone. The solid was then washed three times with water, acetone, and methanol, respectively, and dried under vacuum at 60 °C for 5 h. The Ni2Fe6/UiO-66-$NH_2$-0.4 M solid powder was obtained, and the actual metal content was determined by ICP-OES. Meanwhile, 0.2 and 0.6 M $NaBH_4$ solutions were also used to reduce metal ions in catalyst preparation. The remaining Ni2Fe6/UiO-66-X-y catalysts were prepared in a similar way to that of Ni2Fe6/UiO-66-$NH_2$-0.4 M (y stands for the concentration of $NaBH_4$ solution, 0.2 0.4, and 0.6M). (Note: The theoretical metal loading of the catalysts was 10 wt % by default unless otherwise specified)

**2.3. Characterization.** X-ray diffraction (XRD) patterns were obtained using an Ultima IV X-ray diffractometer (Rigaku Corporation, Japan) with Cu−K$\alpha$ radiation, covering a 2$\theta$ range of 5° to 80°. The functional groups of the samples were analyzed using a scanned Fourier Transform Infrared Spectroscopy (FT-IR) instrument model iS50 (Nicolet Corporation, USA), with wavelengths ranging from 4000 to 400 $cm^{-1}$ and step sizes of 4 $cm^{-1}$. Prior to testing, the powder samples were dried and then pressed with KBr. The morphologies and microstructures of the samples were examined using a JEM-1230 transmission electron microscope (TEM, JEOL, Japan) and a JEM-2010 high-resolution transmission electron microscope (HRTEM, JEOL, Japan), both operated at an accelerating voltage of 200 kV. Elemental distribution analysis was conducted using Scanning Transmission Electron Microscopy (STEM) (FEI-TALOS-F200X) in combination with energy-dispersive X-ray Spectroscopy (EDX) mapping (Super-X). The thermal stability of the samples was assessed using a Pyris 1 thermogravimetric analyzer (TGA, PE, USA) within the temperature range of 50 to 800 °C, employing a heating rate of 10 °C/min under $N_2$ atmosphere. The metal contents of the catalyst were quantitatively determined by using inductively coupled plasma-optical emission spectroscopy (ICP-OES, 730-ES, Varian, Austria). Prior to testing, dissolve, dilute, and filter the catalyst with aqua regia. The textural properties of the samples, including $N_2$ adsorption−desorption behavior at 77 K, The


https://doi.org/10.1021/cbe.4c00108
Chem Bio Eng. 2025, 2, 23−34

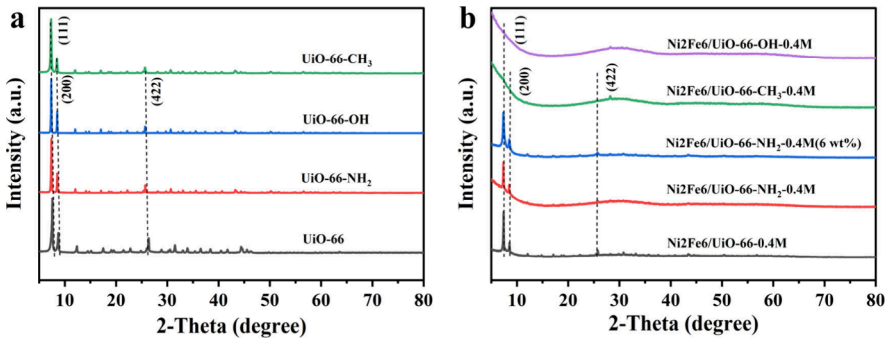


**Figure 1.** XRD patterns of UiO-66-X loaded with MNPs, (a) before and (b) after.

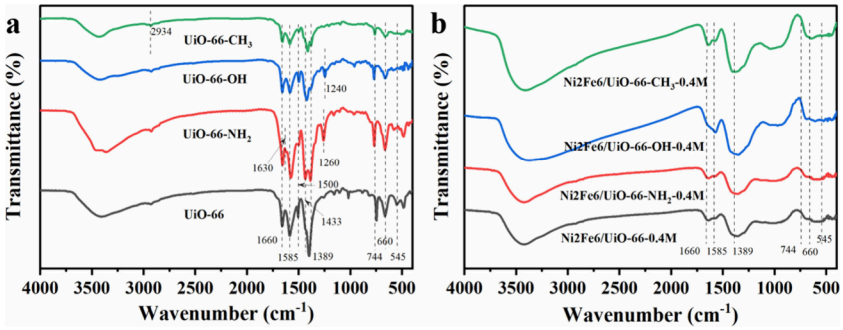


**Figure 2.** FT-IR spectra of UiO-66-X loaded with MNPs, (a) before and (b) after.

Brunauer−Emmett−Teller surface area ($S_{BET}$) and pore size distribution (NLDFT) were studied by a gas adsorption instrument (Autosorb-1-C, Quantachrome, USA). X-ray photoelectron spectroscopy (XPS) measurements were performed by ESCALAB 250Xi (Thermo scientific, UK) equipped with Al K$\alpha$ (1486.6 eV) anode radiation as the excitation source. Temperature-programmed reduction ($H_2$-TPR, Bayer BELCAT-A, Japan) was carried out with the following operating procedures: the catalyst was added into a quartz reactor and reduced with the $H_2$−He gas (50 mL/min) at a temperature rate of 10 °C/min to 300 °C.

**2.4. Catalytic Reaction.** A typical catalytic reaction process was carried out in a 50 mL batch stainless steel autoclave with ML (500 $\mu$L, 2.03 mmol), 1,4-dioxane (20 mL) and catalyst (50 mg). The autoclave was sealed and filled with $H_2$ to 1 MPa for gas exchange for 3 times. The autoclave was then filled with $H_2$ (hydrogen source for the hydrogenation of fatty acid methyl esters) to the desired pressure and heated to the desired temperature with a heat-resistant magnet at a stirring rate of 800 rpm and held for 8 h. After the reaction was completed and the mixture cooled to room temperature, the solution was centrifuged to separate the catalyst. The reaction solution was quantified by gas chromatography GC-FID (Fuli-9790, SE-54 capillary column, 30m × 0.25 mm × 0.25 $\mu$m) using n-hexadecane as internal standard.

The conversion (conversion) of ML and the selectivity (sel.) for the products were calculated as eqs 1 and 2:

$$\text{Conv.} = \frac{\text{moles of ML reacted}}{\text{moles of ML input into the reaction}} \times 100\% \quad (1)$$

$$\text{Sel.} = \frac{\text{moles of product}}{\text{moles of ML reacted}} \times 100\% \quad (2)$$

## 3. RESULTS AND DISCUSSION

**3.1. Catalyst Characterizations.** The crystal structure of the prepared catalysts was analyzed by XRD (Figure 1). UiO-66-X exhibited three distinct diffraction peaks at diffraction angles of $2\theta$ = 7.5°, 8.6° and 25.8°, corresponding to (1 1 1), (2 0 0) and (4 2 2) crystal planes, respectively (Figure 1a).[31,36,37] It suggests that UiO-66-X has similar crystal structures, and the sharp characteristic diffraction peaks indicate the high crystallinity of the synthesized UiO-66-X. The XRD patterns of the Ni2Fe6/UiO-66-X-y catalysts after loading with MNPs exhibited some changes compared to the UiO-66-X (Figure 1b). Specifically, the corresponding XRD characteristic diffraction peaks of UiO-66-OH and UiO-66-$CH_3$ disappeared after the samples were loaded with MNPs. This phenomenon may be attributed to the small size of UiO-66-OH (less than 100 nm, Figure 3c), where the MNPs loading could override the XRD detection signal, resulting in the catalysts exhibiting amorphous characteristics. As for UiO-66 and UiO-66-$NH_2$, their larger sizes (larger than 100 nm, Figure 3a,b) allow them to maintain three distinct diffraction peaks with diffraction angles of $2\theta$ = 7.5°, 8.6°, and 25.8° after loading with MNPs, preserving the crystalline shape of the catalysts. However, Ni2Fe6/UiO-66-$NH_2$-0.4 M exhibited relatively reduced peak intensities compared to Ni2Fe6/UiO-66−0.4M, possibly due to interactions between MNPs and -$NH_2$ groups of UiO-66-$NH_2$.[34] In addition, the characteristic diffraction peaks of Ni and Fe were not detected in the XRD patterns, probably due to the exposure of Ni and Fe to air and water, which resulted in their oxidation to several chemical states, keeping their relative contents below the detection limit of XRD.

Functional groups and chemical bonds in the catalysts before and after MNPs loading were examined via FT-IR (Figure 2). As UiO-66-X is formed through coordination of $Zr^{4+}$ with the organic ligand $H_2$BDC-X, the FT-IR spectra (Figure 2a) display absorption peaks corresponding to aromatic and carboxylic acid groups. The absorption peak at 545 $cm^{-1}$ is associated with the asymmetric stretching vibration of the Zr-(OC) bond in UiO-66-X, while the absorption peak at 660 $cm^{-1}$ is attributed to the asymmetric stretching vibration of the O−Zr−O bond.[34,38,39] The


https://doi.org/10.1021/cbe.4c00108
Chem Bio Eng. 2025, 2, 23−34

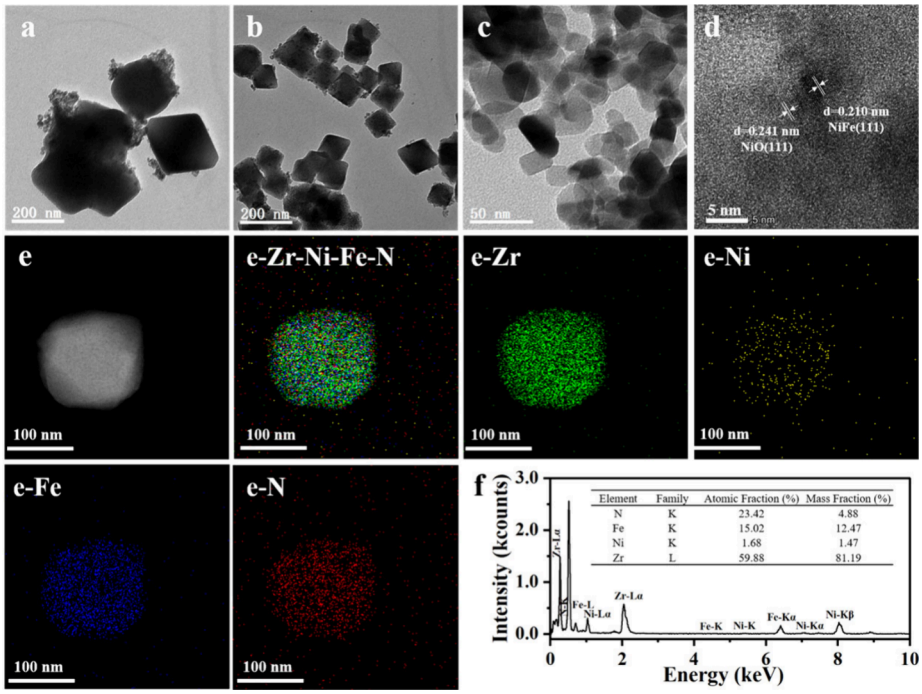


**Figure 3.** TEM images of (a) Ni2Fe6/UiO-66−0.4M, (b) Ni2Fe6/UiO-66-$NH_2$-0.4 M, and (c) Ni2Fe6/UiO-66-OH-0.4M; (d) HRTEM, (e) EDX element mapping, and (f) EDX analysis of (e) of Ni2Fe6/UiO-66-$NH_2$-0.4 M catalyst.

absorption peak at 744 $cm^{-1}$ is attributed to the vibration of −OH in the aromatic acid ligand, while the absorption peak at 1585 $cm^{-1}$ corresponds to the asymmetric stretching vibration of −COOH in the aromatic acid. Additionally, the absorption peaks at 1433 and 1389 $cm^{-1}$ are related to the symmetric stretching vibration of −COOH in the aromatic acid. The peak at 1500 $cm^{-1}$ corresponds to the stretching vibration of the benzene ring, while the strong absorption band in the range of 3000−3700 $cm^{-1}$ is attributed to the stretching vibration of the hydroxyl group of the absorbed water molecule.[36] The ligand UiO-66-$NH_2$ contains a primary amine group bound to the aromatic ring. Two characteristic peaks of the primary amine, attributed to asymmetric and symmetric telescopic vibrations of the N−H bond, respectively, can be detected at 3515 and 3390 $cm^{-1}$. Additionally, a deformation vibration of -$NH_2$ is detected at 1630 $cm^{-1}$, and stretching vibrations between aromatic carbon and nitrogen ($C_{ar}$-N) are observed at 1260 and 1340 $cm^{-1}$.[39,40] The peak of UiO-66-OH at 1240 $cm^{-1}$ is related to the stretching vibration of the C−O bond between the benzene ring and the hydroxyl group.[41,42] The absorption vibration of UiO-66-$CH_3$ at 2934 $cm^{-1}$ is attributed to the formation of −$CH_3$ after the substitution of terephthalic acid by 2-methylterephthalic acid.[37] Compared with the pristine UiO-66-X, the FT-IR absorption peaks of UiO-66-X loaded with MNPs were reduced (Figure 2b), which might be caused by the interaction between MNPs and UiO-66-X, indicating that the chemical environment around UiO-66-X was changed.[43,44]

The morphologies of the Ni2Fe6/UiO-66-X-0.4 M catalysts were observed by TEM (Figure 3). The sizes of UiO-66 and UiO-66-$NH_2$ were larger than 100 nm, and the MNPs on UiO-66 exhibited some agglomeration due to their own magnetism and surface energy (Figure 3a). In contrast, in the case of UiO-66-$NH_2$, the dispersion of MNPs was enhanced (Figure 3b), which might be related to the modification of the support utilizing the -$NH_2$ group. The size of UiO-66-OH was less than 100 nm, and the loading of MNPs might influence its XRD diffraction peaks of the backbone (Figure 3c). Lattice spacing of 0.210 nm and 0.241 were observed in Ni2Fe6/UiO-66-$NH_2$-0.4 M via HRTEM (Figure 3d), corresponding to the Ni−Fe (1 1 1)[45] and NiO (1 1 1)[46] crystal planes, respectively, suggesting the existence of Ni and Fe in multiple chemical states. The elements distribution of Ni2Fe6/UiO-66-$NH_2$-0.4 M was characterized both qualitatively (Figure 3e) and semiquantitatively (Figure 3f) through EDX mapping. Zr and N were respectively derived from the metal node Zr(IV) and the organic ligand 2-amino terephthalic acid of UiO-66-$NH_2$, while Ni and Fe nanoparticles exhibited uniform distribution on UiO-66-$NH_2$.

To ascertain the chemical composition and electronic states of the elements on the surface of the Ni2Fe6/UiO-66-X-0.4 M catalysts, electronic orbital peaks corresponding to Ni 2p and Fe 2p were distinctly detected via XPS (Figure 4), and the binding energy (BE) data subsequent to split-peak fitting were summarized (Table S1). Deconvolution of the Ni 2p orbitals reveals double peaks of spin−orbit splitting for Ni $2p_{3/2}$ (852−

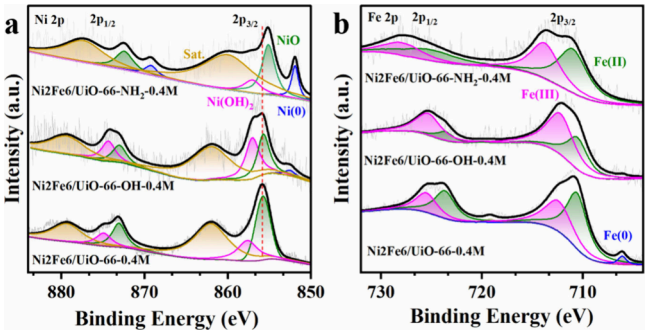


**Figure 4.** XPS peak fitting graph of Ni2Fe6/UiO-66-X-0.4 M catalysts: (a) Ni 2p region and (b) Fe 2p region.


https://doi.org/10.1021/cbe.4c00108
Chem Bio Eng. 2025, 2, 23−34

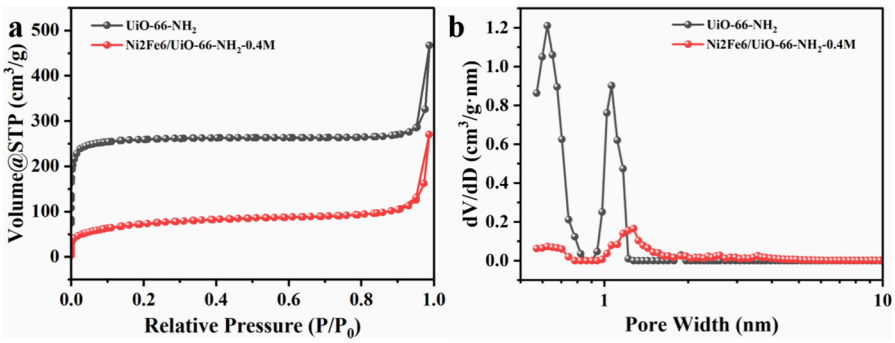


**Figure 5.** UiO-66-$NH_2$ before and after MNPs loading: (a) $N_2$ adsorption−desorption isotherms at 77 K and (b) NLDFT pore size distribution curves.

870 eV) and Ni $2p_{1/2}$ (870−888 eV) (Figure 4a).[12,47] Further detailed identification of Ni $2p_{3/2}$ reveals Ni(0), NiO, $Ni(OH)_2$, and satellite peaks, with Ni species predominantly existing in the oxidized state. When compared to Ni2Fe6/UiO-66−0.4M, the Ni 2p3/2 peaks in Ni2Fe6/UiO-66-$NH_2$-0.4 M and Ni2Fe6/UiO-66-OH-0.4 M catalysts exhibited a shift toward lower BE. This shift was observed despite the MNPs being of identical type and content, and being reduced using a uniform concentration of $NaBH_4$ solution. The negative BE shift can be attributed to variances in functional groups within the support, suggesting that the support may influence the electronic properties of the metal species through metal−support interaction.[31] The electron-donating properties of -$NH_2$ and −OH functional groups interact with the MNPs, facilitating electron transfer from the support to the MNPs, leading to an augmentation in the electron density of the MNPs.[29,48] This electron transfer can substantially enhance the local electronic environment of Ni, thereby contributing to the retention of a higher proportion of Ni(0) within Ni2Fe6/UiO-66-$NH_2$-0.4M.[31,49] Similarly, the Fe 2p spectra can be fitted with peak splitting, revealing the presence of Fe $2p_{3/2}$ (705−718 eV) and Fe $2p_{1/2}$ (718−730 eV) peaks, encompassing Fe(II), Fe(III), and minor portions of Fe(0) (Figure 4b).[12,50] Analogous to the Ni 2p spectra, a slight shift of Fe 2p toward lower BE is observed in Ni2Fe6/UiO-66-$NH_2$-0.4 M and Ni2Fe6/UiO-66-OH-0.4 M catalysts compared to Ni2Fe6/UiO-66−0.4M. These BE shifts of Ni and Fe indicate that the modified chemical microenvironment, influenced by the functional group modification of UiO-66, facilitates electron transfer. The consumption of hydrogen by the Ni2Fe6/UiO-66-$NH_2$-0.4 M catalyst in the temperature range of 50−300 °C was characterized using $H_2$-TPR profile (Figure S1), and the reduction peaks appearing in the low-temperature segment (∼300 °C) could be attributed to NiO species.[51] Furthermore, the actual loadings of Ni and Fe were quantified using ICP-OES (Table S2). A comparison of the theoretical and actual metal contents of Ni2Fe6/UiO-66-$NH_2$-0.4 M catalysts with varying loadings revealed a close correspondence, indicating that liquid-phase impregnation reduction ensured the successful loading of the MNPs into the UiO-66-X supports.

The specific surface area and pore size distribution curves of UiO-66-$NH_2$ before and after loading with MNPs were investigated by employing nitrogen adsorption desorption isotherms (Figure 5). The isotherms of the samples were classified as type I isotherms according to IUPAC (International Union of Pure and Applied Chemistry) (Figure 5a), and the sharp rise in nitrogen adsorption at low relative pressures indicates the microporous nature of the support.[52] The $S_{BET}$ of UiO-66-$NH_2$ was measured to be 1046 $m^2/g$, with total pore volume of 0.72 $cm^3/g$ and average pore size of 2.76 nm (Table 1), which is close to the results reported in the literature.[53]

**Table 1. Pore Structure Parameters of UiO-66-$NH_2$ Loaded with MNPs**

| Sample | $S_{BET}$ ($m^2/g$) | Total pore volume ($cm^3/g$) | Micropore volume ($cm^3/g$) | Average pore diameter (nm) |
|---|---|---|---|---|
| UiO-66-$NH_2$ | 1046 | 0.72 | 0.38 | 2.76 |
| Ni2Fe6/UiO-66-$NH_2$-0.4M | 267 | 0.42 | 0.07 | 6.23 |

After MNPs loading, the $S_{BET}$ of Ni2Fe6/UiO-66-$NH_2$-0.4 M was 267 $m^2/g$ with a total pore volume of 0.07 $cm^3/g$ and average pore size of 6.23 nm. Compared with UiO-66-$NH_2$, Ni2Fe6/UiO-66-$NH_2$-0.4 M showed a significant decrease in $S_{BET}$ and pore volume, suggesting that the MNPs occupied or blocked the cavities of UiO-66-$NH_2$.[34] The increase of average pore size then indicates the presence of mesopores, probably slit mesopores formed by the accumulation of MNPs.[54,55] The pore size distribution of the catalysts was calculated by using the NLDFT model (Figure 5b). It can be seen that UiO-66-$NH_2$ exhibited pore sizes ranging from 0.6 to 1.6 nm. In contrast, the major pore sizes of Ni2Fe6/UiO-66-$NH_2$-0.4 M were reduced due to MNPs occupying or plugging some of the pores, resulting in a reduction of pore sizes smaller than 1 nm and the formation of 2.0−4.0 nm mesopores.

The thermal stability of UiO-66-$NH_2$ before and after loading MNPs was tested by TGA in a nitrogen atmosphere (Figure 6). The weight loss of UiO-66-$NH_2$ within phase 1

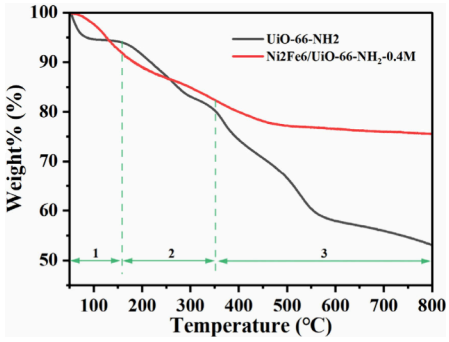


**Figure 6.** TGA curves of the UiO-66-$NH_2$ before and after being loaded with MNPs


https://doi.org/10.1021/cbe.4c00108
Chem Bio Eng. 2025, 2, 23−34

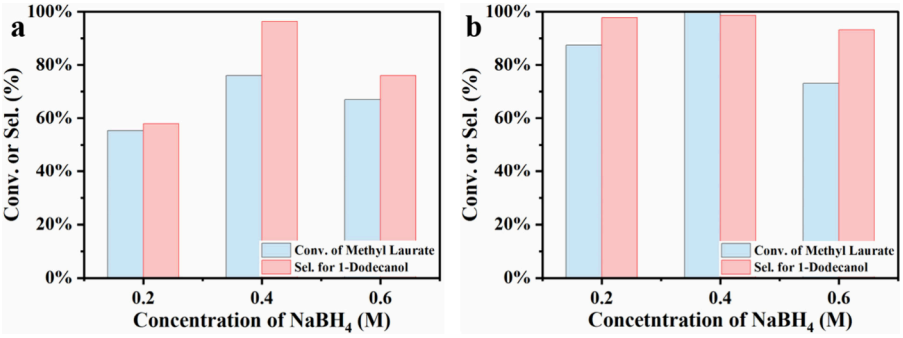


**Figure 7.** Effects of concentrations of $NaBH_4$ solution on catalyst performance: (a) Ni2Fe6/UiO-66 and (b) Ni2Fe6/UiO-66-$NH_2$. Reaction conditions: 0.5 mL ML, 220 °C, 3 MPa $H_2$, 8 h, 50 mg catalyst, 10 wt % metal loading, 20 mL 1,4-dioxane, 800 rpm.

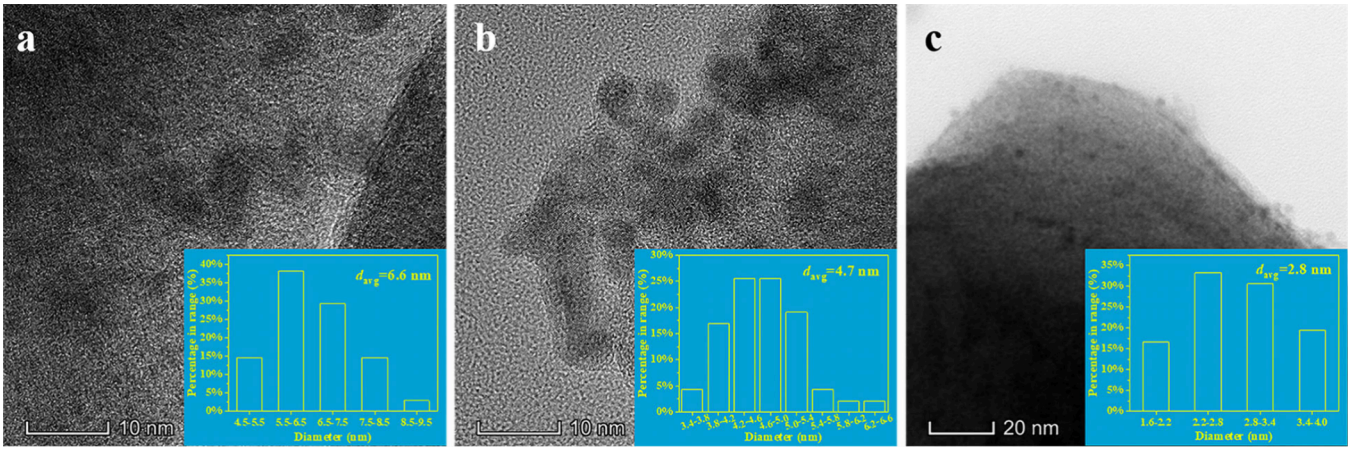


**Figure 8.** TEM images and particle size distributions of Ni2Fe6/UiO-66 catalyst prepared by different concentrations of $NaBH_4$ solution: (a) 0.2 M, (b) 0.4 M, and (c) 0.6 M.

from 50 to 150 °C is attributed to the removal of physically adsorbed water and methanol, the weight loss within phase 2 from 150 to 350 °C is attributed to the removal of residual DMF. During phase 3, which begins at 350 °C, the ligands of UiO-66-$NH_2$ decompose, causing the backbone to collapse, leaving behind $ZrO_2$ as the final solid material.[56,57] For the Ni2Fe6/UiO-66-$NH_2$-0.4 M catalyst, the weight loss process was similar to that of UiO-66-$NH_2$, which was thermally stable up to 350 °C. The successful loading of MNPs was indicated by the variable relative content of residual solids at the end of stage 3, which included $ZrO_2$, Ni, Fe and their oxides.

**3.2. Effects of $NaBH_4$ Solution Concentration on Catalytic Performance of Ni2Fe6/UiO-66-X.** ML was selected as the model reactant to investigate the hydrogenation performance of the catalysts prepared by reducing metal ions using different concentrations of $NaBH_4$ solution (Figure 7). When UiO-66 was employed as the support (Figure 7a), the catalyst prepared using a 0.2 M $NaBH_4$ solution achieved 55.4% conversion of ML and 57.9% selectivity for 1-dodecanol. The main byproducts were lauric acid resulting from hydrogenolysis, with minor quantities of DCN/DCX product n-undecane, as well as the HDO product n-dodecane. With an increase in the concentration of $NaBH_4$ solution to 0.4 M, the conversion of ML reached 76.0%, and the selectivity of 1-dodecanol was 96.4%. However, upon further increasing the $NaBH_4$ solution concentration to 0.6 M, the conversion decreased to 67.1%, the selectivity dropped to 76.2%, and lauric acid is predominant byproduct. The activity of the catalyst exhibited a trend of initially increasing and then decreasing as the concentration of the $NaBH_4$ solution increased. To validate this trend, the catalytic performance test was continued using UiO-66-$NH_2$ as the support (Figure 7b). At a concentration of $NaBH_4$ solution of 0.2 M, the conversion of ML reached 87.4% with a selectivity of 97.8% for 1-dodecanol. Upon increasing the concentration of $NaBH_4$ solution to 0.4 M, the conversion further rose to 99.9%, and the selectivity was 98.6%. However, with a continued increase in the $NaBH_4$ solution concentration to 0.6 M, the conversion and selectivity decreased to 73.1% and 93.2%, respectively, and the byproduct was small amounts of lauric acid.

In order to investigate the reason for the difference in activity, the sizes of the MNPs from the Ni2Fe6/UiO-66 catalysts were observed by TEM (Figure 8). MNPs with average sizes of 6.6 4.7, and 2.8 nm were counted when metal ions were reduced by $NaBH_4$ solutions of 0.2 M (Figure 8a), 0.4 M (Figure 8b), and 0.6 M (Figure 8c), respectively. It could be seen that the sizes of the MNPs became smaller with an increase of the concentration of the $NaBH_4$ solution. It has been shown that the catalytic performance of MNPs is related to their size,[18] and the electron transfer from metal−support interaction is also affected by the particle size.[17] The increase in catalytic activity when the concentration of $NaBH_4$ solution was increased from 0.2 to 0.4 M may be attributed to the decrease in the size of MNPs and the geometric effect dominated the reaction; the decrease in catalytic activity when the concentration of $NaBH_4$ solution was increased to 0.6 M may be attributed to the fact that the activity of the MNPs was affected by both geometric and electronic effects. It has been


https://doi.org/10.1021/cbe.4c00108
Chem Bio Eng. 2025, 2, 23−34

reported that the electronic effect begins to control the activity and selectivity after the particles are smaller than 4 nm, affecting the orbital hybridization and electron transfer between the reactants and the catalytic site, making the activity reversed.[18] Based on these results, a $NaBH_4$ solution of 0.4 M was selected for subsequent studies.

**3.3. Effects of Support Functionalization on Catalytic Performance of Ni2Fe6/UiO-66-X-0.4M.** Ni2Fe6/UiO-66-X-0.4 M catalysts prepared by employing functional group-modified UiO-66-X as support were used for the selective hydrogenation reaction of ML at the concentration of $NaBH_4$ solution of 0.4 M. UiO-66-X have similar structures and crystals, but exhibit different catalytic activities (Figure 9). The conversion of ML could reach 99.9%, and the selectivity for 1-dodecanol was 98.6% when Ni2Fe6/UiO-66-$NH_2$-0.4 M was reacted at 220 °C and 3 MPa $H_2$ for 8 h. Under the same conditions, the conversion of ML catalyzed by Ni2Fe6/UiO-66-$CH_3$-0.4M, Ni2Fe6/UiO-66−0.4M, and Ni2Fe6/UiO-66-OH-0.4 M were 91.2%, 76.0%, and 63.4%, and the selectivities for 1-dodecanol were 97.3%, 96.4%, and 73.8%, respectively.

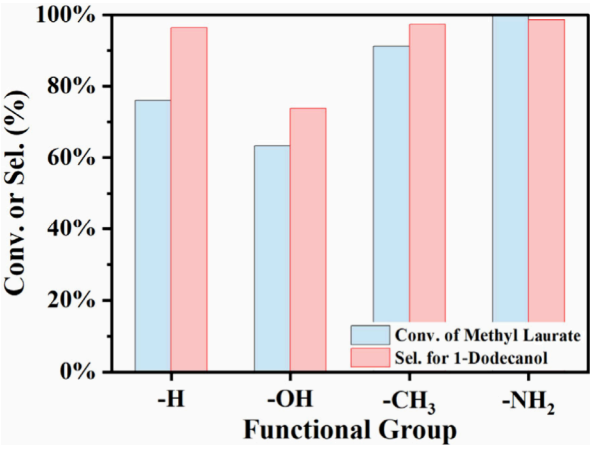


**Figure 9.** Effects of the functional group on catalytic performance. Reaction conditions: 0.5 mL ML, 220 °C, 3 MPa $H_2$, 8 h, 50 mg catalyst, 10 wt % metal loading, 0.4 M $NaBH_4$, 20 mL 1,4-dioxane, 800 rpm.

The superior catalytic performance of -$NH_2$ functionalization in support modification likely stems from its heightened electron-donating capability compared to other functional groups (−OH, −$CH_3$, -H), thereby facilitating increased charge transfer from the functional groups of the support to MNPs.[21,48] This augmentation elevates the charge density surrounding the MNPs, thereby bolstering their stability and catalytic activity. Moreover, as validated by XPS (Figure 4a), the incorporation of -$NH_2$ functionality enhances the reducibility of Ni species to Ni(0), leading to an increased proportion of Ni(0).[21] Consequently, UiO-66-$NH_2$ was chosen as the support, and the catalyst synthesized using a 0.4 M $NaBH_4$ solution was subjected to further investigation in subsequent studies.

**3.4. Effects of Reaction Conditions on Catalytic Performance of Ni2Fe6/UiO-66-$NH_2$-0.4M.** The effect of reaction temperature on the hydrogenation performance of the Ni2Fe6/UiO-66-$NH_2$-0.4 M catalyst was examined (Figure 10a). At 180 °C, the conversion of ML was 17.5% and the selectivity for 1-dodecanol was 88.2%, while lauric acid constituted the primary byproduct. Notably, the reaction rate exhibited a rapid increase with rising temperature. As the temperature was elevated to 220 °C, the conversion and selectivity both reached their optimal values of 99.9% and 98.6%, respectively. However, upon further increasing the temperature to 240 °C, although ML could still be fully reacted

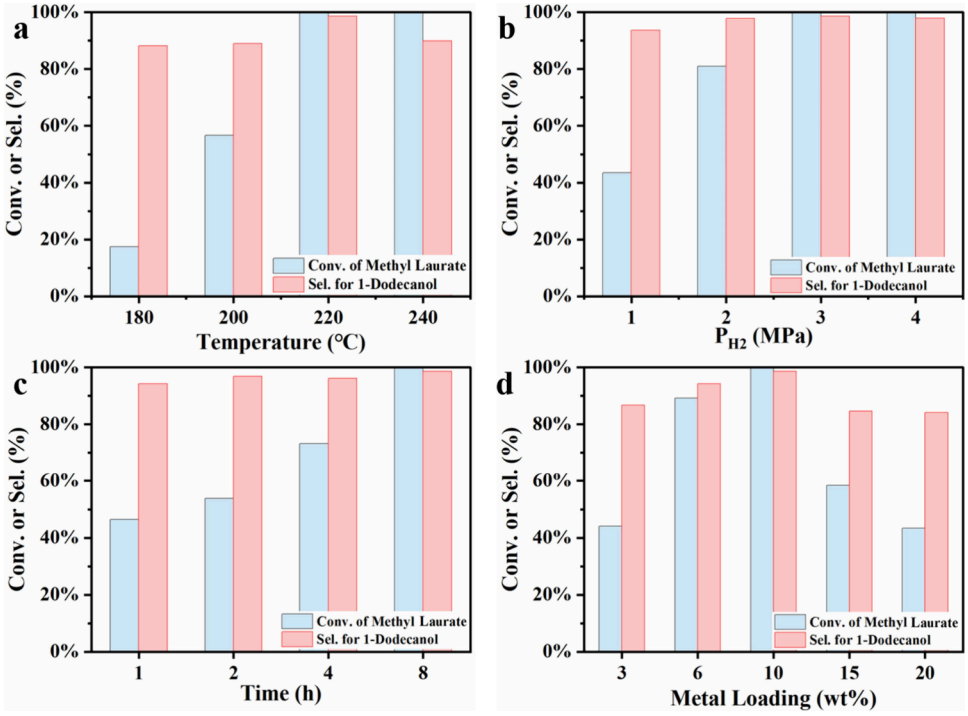


**Figure 10.** Effects of (a) reaction temperature, (b) $H_2$ pressure, (c) time, and (d) metal loading on catalytic performance. Reaction conditions: 0.5 mL ML, 50 mg Ni2Fe6/UiO-66-$NH_2$-0.4M, 20 mL 1,4-dioxane, 800 rpm, (a) 3 MPa $H_2$, 8 h, 10 wt % metal loading, (b) 220 °C, 8 h, 10 wt % metal loading, (c) 220 °C, 3 MPa $H_2$, 10 wt % metal loading (d) 220 °C, 3 MPa $H_2$, 8 h.


https://doi.org/10.1021/cbe.4c00108
Chem Bio Eng. 2025, 2, 23−34

with a conversion maintained at 99.9%, the selectivity for 1-dodecanol decreased to 89.9%, byproducts include n-undecane and n-dodecane were detected in the reaction solution, indicating the occurrence of high-temperature-induced breakage of the C−C and C−OH bonds.

The effect of the $H_2$ pressure on catalyst activity was examined at 220 °C (Figure 10b). At lower $H_2$ pressures, the conversion of ML increased with an increase of $H_2$ pressure from 43.5% at 1 MPa to 99.9% at 3 MPa. Upon further increasing the $H_2$ pressure to 4 MPa, the conversion remained constant at 99.9%. The selectivity for 1-dodecanol also exhibited some dependence on $H_2$ pressure, being 93.7% at 1 MPa and byproducts were alkanes, likely attributed to insufficient hydrogen, leading to the breakage of C−C or C−OH bonds in some reactants. The selectivity for alcohol reached 98.6% when the $H_2$ pressure was increased to 3 MPa, and the hydrogen was sufficient enough to maintain the high selectivity of the reaction. Therefore, an optimum $H_2$ pressure of 3 MPa was chosen.

The conversion and selectivity of the reaction were studied over time at 220 °C and 3 MPa of $H_2$ (Figure 10c). It could be found that the conversion of ML was 46.4% in 1 h and the conversion increased gradually along with the increase of the reaction time. The reactants were completely consumed after 8 h with 99.9% conversion. The selectivity for 1-dodecanol remained above 93.7% throughout the reaction, and the byproducts were minor lauric acid and alkanes.

The effect of metal loading on the reaction process was investigated at 220 °C, 3 MPa of $H_2$, and for 8 h (Figure 10d). At 3 wt % metal loading, the conversion of ML was 44.1% and the selectivity for 1-dodecanol was 86.8%, and the low conversion at this time was caused by insufficient catalytic active sites. With the increase of metal loading lead to active site becomes more and the reaction rate was accelerated. The conversion and selectivity of the reaction were optimized at 10 wt % metal loading with 99.9% and 98.6%, respectively. The conversion decreased with further increase in metal loading. At 20 wt % loading, the conversion of ML was 43.3%, possibly due to reduced catalyst stability resulting from the high loading. Therefore, the optimum metal loading of 10 wt % was determined. The catalytic results were also compared to other reported studies (Table S3).

**3.5. Kinetic Study.** Since the hydrogenation reaction on the ML in the Ni2Fe6/UiO-66-$NH_2$-0.4 M catalyst is a heterogeneous reaction, the reaction kinetics may be affected by diffusion limitations. Therefore, the Weisz-Prater criterion and the Mears criterion were used to analyze the effects of internal and external diffusion, respectively.[58,59]

If the Weisz-Prater parameter ($C_{WP}$) is less than 1, it indicates that the effects of internal diffusion can be neglected,and the $C_{WP}$ is calculated using eq 3.[58,59] The hydrogenation reaction of fatty acid methyl esters is considered a first-order irreversible reaction.[16] Based on the lowest reaction temperature used in this study (180 °C), the $C_{WP}$ for the hydrogenation of ML on the Ni2Fe6/UiO-66-$NH_2$-0.4 M catalyst was calculated. In this calculation, $-r_A$ represents the observed reaction rate, which is derived from the data at 180 °C after 8 h of reaction (Figure 10a), and is $2.47 \times 10^{-7}$ mol/$g_{catalyst}$/s. The catalyst density ($\rho_c$) is calculated to be 1.35 g/cm$^3$, based on the mass ratio of the metal components and the support in the Ni2Fe6/UiO-66-$NH_2$-0.4 M catalyst, as determined by ICP-OES (Table S2). The radius of the catalyst particles ($R_c$) is determined to be 0.05 mm, based on TEM analysis (Figure 3), which shows that the particles are all smaller than 0.1 mm. $C_{AS}$ is the concentration of reactants on the surface of the catalyst, and an average concentration value of $5.08 \times 10^{-2}$ mol/L was taken. $D_e$ is the effective diffusion coefficient of reactants (m$^2$/s) and is calculated according to eq 4.[58]

$$C_{WP} = \frac{-r_A \rho_c R_c^2}{D_e C_{AS}} < 1 \tag{3}$$

$$D_e = \frac{D_{AB} \Phi_P \sigma}{\tilde{\tau}} \tag{4}$$

$$D_{AB} = 7.48 \times 10^{-8} \frac{(\varphi M_B)^{1/2} T}{\eta_B V_A^{0.6}} \tag{5}$$

In eq 4, $\Phi_p$, $\sigma$, and $\tilde{\tau}$ are the porosity, constriction factor, and tortuosity of the catalyst particles, which generally take the values of 0.4, 0.8, and 3.0, respectively.[59] $D_{AB}$ is the diffusion coefficient (m$^2$/s) of solute A (ML) in solvent B (1,4-dioxane), which in dilute solution can be calculated according to the Wilke-Chang eq 5.[58,60] $\varphi$ is the association factor of solvent B, which is taken as 1.0. $M_B$ represents the relative molecular mass of solvent B, which is 88.11 kg/kmol. $T$ is the reaction temperature, which is 453.15 K. $\eta_B$ denotes the viscosity of solvent B, which is 0.64 mPa·s. $V_A$ stands for the molar volume of solute A (ML) at normal boiling point, which is 306.8 cm$^3$/mol.[61] The $D_{AB}$ and $D_e$ were calculated to be $1.60 \times 10^{-9}$ m$^2$/s and $1.71 \times 10^{-10}$, respectively, and the $C_{WP}$ was 0.10 less than 1. Therefore, the effect of internal diffusion can be neglected in the kinetic study.

If the Mears parameter ($C_M$) is less than 0.15, it means that the effect of external diffusion can be neglected, and the $C_M$ is calculated according to eq 6.[59] $-r_A$ and $R_c$ take the same values as the Weisz-Prater criterion, and n is the number of reaction orders that is 1. $\rho_b$ is the bulk density of the catalyst, calculated according to eq 7.[59] $k_c$ is the mass transfer coefficient, and is calculated according to eq 8. $Sh$ is the Sherwood number is valued as 2,[62] and $D_{AB}$ is calculated as in eq 5. $d_c$ is the diameter of the catalyst particles and is taken as 0.1 mm. $C_{Ab}$ is the bulk concentration of the reactant and is estimated to be $5.08 \times 10^{-2}$ mol/L using the average of the concentrations. $k_c$ and $\rho_b$ were calculated to be $3.20 \times 10^{-5}$ m/s and 0.81 g/cm$^3$, respectively, with a $C_M$ of $0.06 \times 10^{-2}$ less than 0.15, and the reaction was also carried out at a high stirring speed (800 rpm). Therefore, the effect of external diffusion can be neglected in the kinetic study.

$$C_M = \frac{-r_A \rho_b R_c n}{k_c C_{Ab}} < 0.15 \tag{6}$$

$$\rho_b = (1 - \Phi p)\rho_c \tag{7}$$

$$k_c = \frac{Sh D_{AB}}{d_c} \tag{8}$$

The kinetics of the reaction was studied after excluding the effect of diffusion. The catalytic results of Ni2Fe6/UiO-66-$NH_2$-0.4 M in the range 190−230 °C at low conversion (Figure S3) were used for the kinetic analysis of the reaction to calculate the reaction rate ($r$) and further to obtain the apparent activation energy ($E_a$) by the Arrhenius formula. $r$ and $E_a$ were calculated as eqs 9 and 10.[63,64] $\Delta n$ is the molar amount of the reaction transformation (mmol), $m_c$ is the mass


https://doi.org/10.1021/cbe.4c00108
Chem Bio Eng. 2025, 2, 23−34

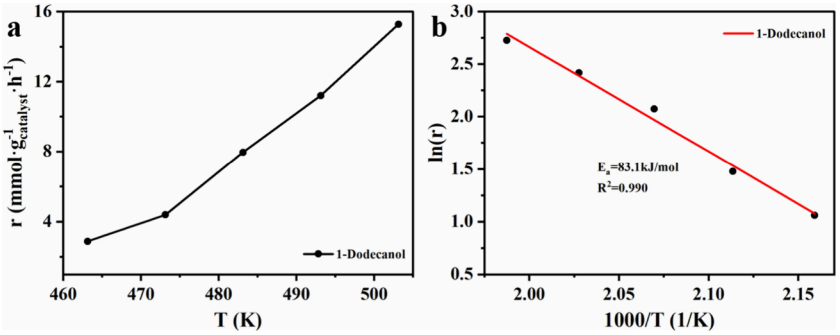


**Figure 11.** Kinetic study: (a) reaction rates of Ni2Fe6/UiO-66-$NH_2$-0.4 M catalyst for the production of 1-hexadecanol at different temperatures; (b) reaction rate constant for Arrhenius plots.

of the catalyst (g), $t$ is the reaction time (h), and $T$ is the reaction temperature (K).

$$r = \frac{\Delta n}{m_c t} \tag{9}$$

$$\ln r = -\frac{E_a}{RT} + \ln A \tag{10}$$

The reaction rates of the Ni2Fe6/UiO-66-$NH_2$-0.4 M catalyst at different temperatures were investigated (Figure 11a), and it could be seen that the production rate of 1-dodecanol accelerated as the reaction temperature increased. The $E_a$ was determined by using the Arrhenius formula and fitting the 1000/T-ln(r) curve relationship (Figure 11b), which gave a value of 83.1 kJ/mol for the production of 1-dodecanol.

**3.6. Reaction Mechanism.** The hydrogenation mechanism of fatty acid methyl esters is influenced by the metal properties and the support, and fatty acid methyl esters can be adsorbed on the metal surface of the catalysts in the $\eta^1$(C)-acyl and $\eta^2$(C, O)-aldehyde configurations.[10,14,15] In metal catalysts with low oxophilicity, such as noble metals and Ni, reactants tend to adsorb to the metal surface in the $\eta^1$(C)-acyl conformation, which tends to cause C−C bond breaking to generate alkanes in the DCN/DCX process.[10,65] In contrast, the $\eta^2$(C, O)-aldehyde configuration formed by doping moderately oxophilic metals such as Fe, Zn, and Mo inhibits C−C bond breaking and promotes C−O bond breaking, which facilitates the generation of alcohols.[16] Studies of Ni−In,[16] Ni−Fe,[12] Ni−Zn,[15] and Pt−Zn[66] similarly support the $\eta^2$(C, O)-aldehyde configuration. The Ni2Fe6/UiO-66-$NH_2$-0.4 M catalyst showed promising selectivity for fatty alcohols, and thus it was concluded that ML adsorbed in the $\eta^2$(C, O)-aldehyde conformation on the metal surface of Ni2Fe6/UiO-66-NH2−0.4 M to undergo the reaction.

Based on the results of catalyst characterization and performance evaluation, the catalytic mechanism of Ni2Fe6/UiO-66-$NH_2$-0.4 M was discussed (Figure 12). It was confirmed by HRTEM that Ni and Fe in Ni2Fe6/UiO-66-$NH_2$-0.4 M are mainly present as oxides and Ni−Fe. It is reported that $H_2$ is easily cleaved on Ni species to form H atoms,[16] and the low oxophilicity of Ni and the moderate oxophilicity of Fe allow fatty acid esters to adsorb onto the metal surfaces via $\eta^2$(C, O)-aldehyde conformation.[10] The surface-functionalized UiO-66-$NH_2$ support allows efficient electron transfer from -$NH_2$ with electron-donating properties to MNPs with a size of 4.7 nm, and this metal−support interaction stabilizes the catalytic activity of the MNPs. Under the action of the catalyst, the $R_1CO^*$ intermediate was obtained by breaking the C−O bond of the ester group and combined with the H atom to generate the intermediate aliphatic aldehyde. The C═O bond of the aliphatic aldehyde was similarly adsorbed on the metal surface via the $\eta^2$(C, O)-aldehyde conformation, and the C═O bond is rapidly hydrogenated to produce fatty alcohol.

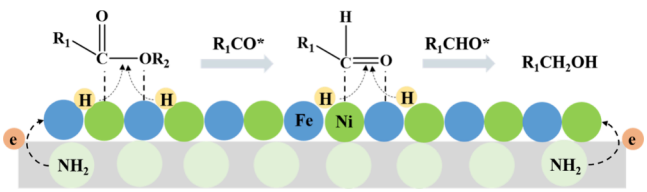


**Figure 12.** Probable catalytic mechanism of fatty acid esters catalyzed by Ni2Fe6/UiO-66-$NH_2$-0.4 M ($R_1$, $R_2$ represent alkyl groups).

**3.7. Recycling and Versatility Performance.** In order to investigate the recycling stability of the 10 wt % Ni2Fe6/UiO-66-NH2−0.4 M catalyst, recycling tests were carried out by reacting at 220 °C and 3 MPa $H_2$ for 8 h (Figure 13) and 1 h (Figure S4). It could be seen that the conversion of ML decreased from 99.9% in the first run to 89.7% in the fifth run, and the selectivity of 1-dodecanol was maintained over 94.8%, which proves the reliability of the catalyst. The TEM image of the catalyst after five runs (Figure S2a) revealed certain loosening of the backbone, which may be attributed to the prolonged operation at high temperature and pressure,

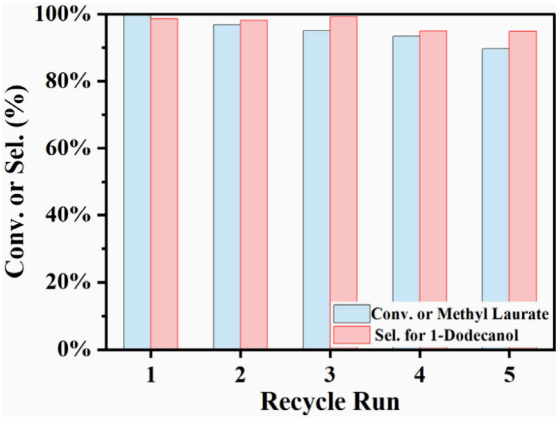


**Figure 13.** Recycling run performance of Ni2Fe6/UiO-66-$NH_2$-0.4M-catalyzed. Reaction conditions: 0.5 mL ML, 50 mg catalyst, 3 MPa $H_2$, 220 °C, 20 mL 1,4-dioxane, 8 h, 800 rpm


https://doi.org/10.1021/cbe.4c00108
Chem Bio Eng. 2025, 2, 23−34

Table 2. Ni2Fe6/UiO-66-$NH_2$-0.4M-Catalyzed Selective Hydrogenation of Fatty Acid Methyl Esters to Alcohols[a]

| Entry | Reactant | Conv. (%) | Sel. for R-OH (%) |
|---|---|---|---|
| 1 | 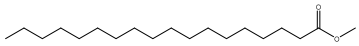 Methyl Stearate | 97.9 | 95.4 |
| 2 | 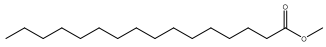 Methyl Palmitate | 97.6 | 96.1 |
| 3 | 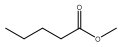 Methyl Valerate [b] | 98.2 | 94.4 |

[a]Reaction conditions: 500 mg reactant, 50 mg catalyst, 3 MPa $H_2$, 220 °C, 20 mL 1,4-dioxane, 8 h, 800 rpm. [b]500 mLof reactant.

resulting in a decrease in catalytic activity. Meanwhile, the statistical analysis of the metals in the catalyst showed that the average size of the metal particles increased to 8.8 nm (Figure S2b), which could be attributed to the high temperature and the reaction environment of the reducing hydrogen that caused the metal particles to sinter and agglomerate, which led to an increase in the size and caused a decrease in the stability of the catalysts during the recycling runs.[67] Furthermore, the catalyst was evaluated for its versatility in catalyzing fatty acid methyl esters with different carbon chain lengths (Table 2), and the catalyst showed good catalytic activity for methyl valerate, methyl palmitate, and methyl stearate.

## 4. CONCLUSION

To reduce the cost associated with noble metals, the catalytic hydrogenation activity of Ni2Fe6/UiO-66 was enhanced through two strategies: control of the MNPs size and modification of support functionalization. Ni2Fe6/UiO-66-X-y catalysts were then prepared via a liquid-phase impregnation reduction method. TEM and HRTEM demonstrated that the concentration of $NaBH_4$ solution can significantly affect the size of MNPs, as evidenced by the fact that high concentration helps to prepare smaller-sized MNPs, and the best catalytic effect was achieved with the average size of 4.7 nm prepared at 0.4 M $NaBH_4$ solution concentration. FT-IR and XPS demonstrated that functionalization of the support could promote the electron transfer between the MNPs and the support, the metal−support interaction formed could help to improve the activity of the catalysts, and the best effect was achieved with the modification by the -$NH_2$ group. The effects of reaction conditions on the performance of Ni2Fe6/UiO-66-$NH_2$-0.4 M catalyst were investigated, which showed ML conversion of 99.9% and 1-dodecanol selectivity of 98.6% at 220 °C and 3 MPa $H_2$ for 8 h. Meanwhile, a catalytic mechanism based on metal−support interaction was explored, wherein the reactants were adsorbed on the surface of MNPs via the $\eta^2$(C, O)-aldehyde configuration, promoting the generation of fatty alcohol. Furthermore, the Ni2Fe6/UiO-66-$NH_2$-0.4 M catalyst allowed for five stable recycling runs and was catalytically versatile for other fatty acid methyl esters.

## ■ ASSOCIATED CONTENT

### Supporting Information

The Supporting Information is available free of charge at https://pubs.acs.org/doi/10.1021/cbe.4c00108.

Materials; TEM image; ICP-OES and XPS analytical table (PDF)

## ■ AUTHOR INFORMATION


### Corresponding Author

**Gang Xu** − *College of Chemical and Biological Engineering, Zhejiang University, Hangzhou 310058, China;* orcid.org/0000-0001-8516-8731; Email: xugang_1030@zju.edu.cn

### Authors

**Pengcheng Li** − *College of Chemical and Biological Engineering, Zhejiang University, Hangzhou 310058, China*

**Tianyu Ma** − *College of Chemical and Biological Engineering, Zhejiang University, Hangzhou 310058, China*

**Youyang Wu** − *College of Chemical and Biological Engineering, Zhejiang University, Hangzhou 310058, China*

**Jianping Wu** − *College of Chemical and Biological Engineering, Zhejiang University, Hangzhou 310058, China;* orcid.org/0000-0002-9924-7307

**Haoran Yu** − *College of Chemical and Biological Engineering, Zhejiang University, Hangzhou 310058, China;* orcid.org/0000-0001-9012-4688

**Lirong Yang** − *College of Chemical and Biological Engineering, Zhejiang University, Hangzhou 310058, China;* orcid.org/0000-0002-6378-8451

Complete contact information is available at: https://pubs.acs.org/10.1021/cbe.4c00108


### Author Contributions

**Pengcheng Li:** Conceptualization, Data curation, Formal analysis, Methodology, Investigation, Software, Writing-Original draft preparation, Writing-Review & Editing. **Tianyu Ma**: Methodology, Investigation, Software, Writing-Review. **Youyang Wu:** Investigation, Writing-Review. **Jianping Wu**: Methodology, Investigation. **Haoran Yu**: Methodology, Investigation. **Lirong Yang**: Methodology. **Gang Xu**: Supervision, Project administration, Conceptualization, Data curation, Formal analysis, Methodology, Writing-Original draft preparation, Writing-Review & Editing.

### Notes

The authors declare no competing financial interest.

## ■ ACKNOWLEDGMENTS

The authors would like to thank for the financial support provided by the National Natural Science Foundation of China (21878264) and the National Key R&D Program of China (2019YFA09005000).

## REFERENCES


(1) Zhou, Y.; Remón, J.; Jiang, Z.; Matharu, A. S.; Hu, C. Tuning the Selectivity of Natural Oils and Fatty Acids/Esters Deoxygenation to Biofuels and Fatty Alcohols: A Review. *Green Energy Environ.* **2023**, *8* (3), 722−743.

(2) Qu, R.; Junge, K.; Beller, M. Hydrogenation of Carboxylic Acids, Esters, and Related Compounds over Heterogeneous Catalysts: A Step toward Sustainable and Carbon-Neutral Processes. *Chem. Rev.* **2023**, *123* (3), 1103−1165.

(3) Strekalova, A. A.; Shesterkina, A. A.; Kustov, L. M. Recent Progress in Hydrogenation of Esters on Heterogeneous Bimetallic Catalysts. *Catal. Sci. Technol.* **2021**, *11* (22), 7229−7238.

(4) Sánchez, M. A.; Torres, G. C.; Mazzieri, V. A.; Pieck, C. L. Selective Hydrogenation of Fatty Acids and Methyl Esters of Fatty Acids to Obtain Fatty Alcohols−a Review. *J. Chem. Technol. Biotechnol.* **2017**, *92* (1), 27−42.

(5) Ding, S.; Parlett, C. M. A.; Fan, X. Recent Developments in Multifunctional Catalysts for Fatty Acid Hydrodeoxygenation as a Route towards Biofuels. *Mol. Catal.* **2022**, *523*, No. 111492.

(6) Taniguchi, S.; Makino, T.; Watanuki, H.; Kojima, Y.; Sano, M.; Miyake, T. Effect of Pt Addition to Ru−Sn/$Al_2O_3$ Catalyst on Hydrogenation of Methyl Laurate. *Appl. Catal. Gen.* **2011**, *397* (1), 171−173.

(7) Huang, C.; Zhang, H.; Zhao, Y.; Chen, S.; Liu, Z. Diatomite-Supported Pd−M (M = Cu, Co, Ni) Bimetal Nanocatalysts for Selective Hydrogenation of Long-Chain Aliphatic Esters. *J. Colloid Interface Sci.* **2012**, *386* (1), 60−65.

(8) Van Deelen, T. W.; Hernández Mejía, C.; De Jong, K. P. Control of Metal-Support Interactions in Heterogeneous Catalysts to Enhance Activity and Selectivity. *Nat. Catal.* **2019**, *2* (11), 955−970.

(9) Han, B.; Yu, B.; Wang, J.; Liu, M.; Gao, G.; Xia, K.; Gao, Q.; Zhou, C. Understanding the Electronic Metal-Support Interactions of the Supported Ni Cluster for the Catalytic Hydrogenation of Ethylene. *Mol. Catal.* **2021**, *511*, No. 111731.

(10) Žula, M.; Grilc, M.; Likozar, B. Hydrocracking, Hydrogenation and Hydro-Deoxygenation of Fatty Acids, Esters and Glycerides: Mechanisms, Kinetics and Transport Phenomena. *Chem. Eng. J.* **2022**, *444*, No. 136564.

(11) Long, F.; Wu, S.; Chen, H.; Jia, S.; Cao, X.; Liu, P.; Lu, Y.; Jiang, J.; Zhang, X.; Xu, J. Alcohol Production from Fatty Acids via $Ni_3Fe$/Rutile: Revealing the Role of Oxygen Vacancy and Metal-Support Electronic Density Characteristics. *J. Catal.* **2023**, *428*, No. 115171.

(12) Kong, X.; Fang, Z.; Bao, X.; Wang, Z.; Mao, S.; Wang, Y. Efficient Hydrogenation of Stearic Acid over Carbon Coated NiFe Catalyst. *J. Catal.* **2018**, *367*, 139−149.

(13) Kepp, K. P. A Quantitative Scale Ofoxophilicity and Thiophilicity. *Inorg. Chem.* **2016**, *55* (18), 9461−9470.

(14) Mavrikakis, M.; Barteau, M. A. Oxygenate Reaction Pathways on Transition Metal Surfaces. *J. Mol. Catal. Chem.* **1998**, *131* (1), 135−147.

(15) Pan, Z.; Wang, R.; Chen, J. Deoxygenation of Methyl Laurate as a Model Compound on Ni-Zn Alloy and Intermetallic Compound Catalysts: Geometric and Electronic Effects of Oxophilic Zn. *Appl. Catal. B Environ.* **2018**, *224*, 88−100.

(16) Wang, L.; Niu, X.; Chen, J. $SiO_2$ Supported Ni-In Intermetallic Compounds: Efficient for Selective Hydrogenation of Fatty Acid Methyl Esters to Fatty Alcohols. *Appl. Catal. B Environ.* **2020**, *278*, No. 119293.

(17) Liu, L.; Corma, A. Metal Catalysts for Heterogeneous Catalysis: From Single Atoms to Nanoclusters and Nanoparticles. *Chem. Rev.* **2018**, *118* (10), 4981−5079.

(18) Wang, H.; Gu, X.-K.; Zheng, X.; Pan, H.; Zhu, J.; Chen, S.; Cao, L.; Li, W.-X.; Lu, J. Disentangling the Size-Dependent Geometric and Electronic Effects of Palladium Nanocatalysts beyond Selectivity. *Sci. Adv.* **2019**, *5*, No. eaat6413.

(19) Li, W.; Guo, Z.; Yang, J.; Li, Y.; Sun, X.; He, H.; Li, S.; Zhang, J. Advanced Strategies for Stabilizing Single-Atom Catalysts for Energy Storage and Conversion. *Electrochem. Energy Rev.* **2022**, *5* (3), 9.

(20) Zhou, J.; Gao, Z.; Xiang, G.; Zhai, T.; Liu, Z.; Zhao, W.; Liang, X.; Wang, L. Interfacial Compatibility Critically Controls Ru/$TiO_2$ Metal-Support Interaction Modes in $CO_2$ Hydrogenation. *Nat. Commun.* **2022**, *13* (1), 327.

(21) Phan, D.-P.; Le, V. N.; Nguyen, T. H.; Kim, H. B.; Park, E. D.; Kim, J.; Lee, E. Y. Effect of Amino-Defective-MOF Materials on the Selective Hydrodeoxygenation of Fatty Acid over Pt-Based Catalysts. *J. Catal.* **2021**, *400*, 283−293.

(22) Chen, D.; Yang, W.; Jiao, L.; Li, L.; Yu, S.; Jiang, H. Boosting Catalysis of Pd Nanoparticles in MOFs by Pore Wall Engineering: The Roles of Electron Transfer and Adsorption Energy. *Adv. Mater.* **2020**, *32* (30), No. 2000041.

(23) Marakatti, V. S.; Peter, S. C. Synthetically Tuned Electronic and Geometrical Properties of Intermetallic Compounds as Effective Heterogeneous Catalysts. *Prog. Solid State Chem.* **2018**, *52*, 1−30.

(24) Qian, Y.; Zhang, F.; Pang, H. A Review of MOFs and Their Composites-Based Photocatalysts: Synthesis and Applications. *Adv. Funct. Mater.* **2021**, *31* (37), No. 2104231.

(25) Yang, Q.; Xu, Q.; Jiang, H.-L. Metal−Organic Frameworks Meet Metal Nanoparticles: Synergistic Effect for Enhanced Catalysis. *Chem. Soc. Rev.* **2017**, *46* (15), 4774−4808.

(26) Al Obeidli, A.; Ben Salah, H.; Al Murisi, M.; Sabouni, R. Recent Advancements in MOFs Synthesis and Their Green Applications. *Int. J. Hydrog. Energy* **2022**, *47* (4), 2561−2593.

(27) Cavka, J. H.; Jakobsen, S.; Olsbye, U.; Guillou, N.; Lamberti, C.; Bordiga, S.; Lillerud, K. P. A New Zirconium Inorganic Building Brick Forming Metal Organic Frameworks with Exceptional Stability. *J. Am. Chem. Soc.* **2008**, *130* (42), 13850−13851.

(28) Bai, Y.; Dou, Y.; Xie, L.-H.; Rutledge, W.; Li, J.-R.; Zhou, H.-C. Zr-Based Metal−Organic Frameworks: Design, Synthesis, Structure, and Applications. *Chem. Soc. Rev.* **2016**, *45* (8), 2327−2367.

(29) Wang, H.; Liu, X.; Yang, W.; Mao, G.; Meng, Z.; Wu, Z.; Jiang, H.-L. Surface-Clean $Au_{25}$ Nanoclusters in Modulated Microenvironment Enabled by Metal−Organic Frameworks for Enhanced Catalysis. *J. Am. Chem. Soc.* **2022**, *144* (48), 22008−22017.

(30) Feng, X.; Jena, H. S.; Krishnaraj, C.; Leus, K.; Wang, G.; Chen, H.; Jia, C.; Van Der Voort, P. Generating Catalytic Sites in UiO-66 through Defect Engineering. *ACS Appl. Mater. Interfaces* **2021**, *13* (51), 60715−60735.

(31) Guo, M.; Wang, F.; Zhang, M.; Wang, L.; Zhang, X.; Li, G. Modulating Pt Nanoparticles Confined in UiO-66 by Linker Functional Groups for Controllable Hydrogenation. *J. Catal.* **2023**, *424*, 221−235.

(32) Geng, R.; Jia, H.; Xie, Y.; Pan, D.; Yu, F.; Fan, B. Influence of the Defects on Selective Hydrogenation of Cinnamaldehyde to Cinnamyl Alcohol over UiO-66 Supported Pt Catalysts. *Microporous Mesoporous Mater.* **2022**, *338*, No. 111968.

(33) Yeh, B.; Vicchio, S. P.; Chheda, S.; Zheng, J.; Schmid, J.; Löbbert, L.; Bermejo-Deval, R.; Gutiérrez, O. Y.; Lercher, J. A.; Lu, C. C.; Neurock, M.; Getman, R. B.; Gagliardi, L.; Bhan, A. Site Densities, Rates, and Mechanism of Stable Ni/UiO-66 Ethylene Oligomerization Catalysts. *J. Am. Chem. Soc.* **2021**, *143* (48), 20274−20280.

(34) Guan, Q.; Wang, B.; Chai, X.; Liu, J.; Gu, J.; Ning, P. Comparison of Pd-UiO-66 and Pd-UiO-66-$NH_2$ Catalysts Performance for Phenol Hydrogenation in Aqueous Medium. *Fuel* **2017**, *205*, 130−141.

(35) Li, P.; Zhang, M.; Wang, S.; Yu, H.; Wu, J.; Yang, L.; Xu, G. Pd−Ni−Fe Nanoparticles Supported on UiO-66 for Selective Hydrogenation of Fatty Acid Methyl Esters to Alcohols. *ACS Appl. Nano Mater.* **2023**, *6* (20), 18892−18904.

(36) Man, Z.; Meng, Y.; Lin, X.; Dai, X.; Wang, L.; Liu, D. Assembling UiO-66@$TiO_2$ Nanocomposites for Efficient Photocatalytic Degradation of Dimethyl Sulfide. *Chem. Eng. J.* **2022**, *431*, No. 133952.

(37) Li, P.; Lin, F.; Feng, D.; Zhang, X.; Feng, Y. Using Surface-Modified UiO-66 with Hierarchical Pores to Pack Polyethylene Glycol for Phase Change Thermal Energy Storage: Experiment and Molecular Dynamics Simulations. *J. Energy Storage* **2022**, *55*, No. 105806.

(38) Wang, C.; Li, A.-R.; Ma, Y.-L. Phosphomolybdic Acid Niched in the Metal-Organic Framework UiO-66 with Defects: An Efficient and Stable Catalyst for Oxidative Desulfurization. *Fuel Process. Technol.* **2021**, *212*, No. 106629.
(39) Kandiah, M.; Usseglio, S.; Svelle, S.; Olsbye, U.; Lillerud, K. P.; Tilset, M. Post-Synthetic Modification of the Metal−Organic Framework Compound UiO-66. *J. Mater. Chem.* **2010**, *20* (44), 9848−9851.
(40) Lin, K.-Y. A.; Liu, Y.-T.; Chen, S.-Y. Adsorption of Fluoride to UiO-66-$NH_2$ in Water: Stability, Kinetic, Isotherm and Thermodynamic Studies. *J. Colloid Interface Sci.* **2016**, *461*, 79−87.
(41) Xin, Y.; Wang, D.; Yao, D.; Ning, H.; Li, X.; Ju, X.; Zhang, Y.; Yang, Z.; Xu, Y.; Zheng, Y. Post-Synthetic Modification of UiO-66-OH toward Porous Liquids for CO2 Capture. *New J. Chem.* **2022**, *46* (5), 2189−2197.
(42) Rada, Z. H.; Abid, H. R.; Shang, J.; Sun, H.; He, Y.; Webley, P.; Liu, S.; Wang, S. Functionalized UiO-66 by Single and Binary $(OH)_2$ and $NO_2$ Groups for Uptake of $CO_2$ and $CH_4$. *Ind. Eng. Chem. Res.* **2016**, *55* (29), 7924−7932.
(43) Zhang, J.; Guo, Z.; Yang, Z.; Wang, J.; Xie, J.; Fu, M.; Hu, Y. $TiO_2$@UiO-66 Composites with Efficient Adsorption and Photocatalytic Oxidation of VOCs: Investigation of Synergistic Effects and Reaction Mechanism. *ChemCatChem.* **2021**, *13* (2), 581−591.
(44) Song, M.; Liu, T.; Hong, X.; Liu, G. Coordination Environment Dependent Surface Cu State for CO2 Hydrogenation to Methanol. *ACS Sustain. Chem. Eng.* **2023**, *11* (32), 12135−12144.
(45) Zhao, J.; Guo, X.; Shi, R.; Waterhouse, G. I. N.; Zhang, X.; Dai, Q.; Zhang, T. NiFe Nanoalloys Derived from Layered Double Hydroxides for Photothermal Synergistic Reforming of $CH_4$ with $CO_2$. *Adv. Funct. Mater.* **2022**, *32* (31), No. 2204056.
(46) Zhao, L.; Zhang, Y.; Zhao, Z.; Zhang, Q.; Huang, L.; Gu, L.; Lu, G.; Hu, J.; Wan, L. Steering Elementary Steps towards Efficient Alkaline Hydrogen Evolution via Size-Dependent Ni/NiO Nanoscale Heterosurfaces. *Natl. Sci. Rev.* **2020**, *7* (1), 27−36.
(47) Chen, L.; Lu, L.; Zhu, H.; Chen, Y.; Huang, Y.; Li, Y.; Wang, L. Improved Ethanol Electrooxidation Performance by Shortening Pd−Ni Active Site Distance in Pd−Ni−P Nanocatalysts. *Nat. Commun.* **2017**, *8* (1), 1−9.
(48) Yin, Y.; Lv, R.; Zhang, W.; Lu, J.; Ren, Y.; Li, X.; Lv, L.; Hua, M.; Pan, B. Exploring Mechanisms of Different Active Species Formation in Heterogeneous Fenton Systems by Regulating Iron Chemical Environment. *Appl. Catal. B Environ.* **2021**, *295*, No. 120282.
(49) Shi, W.; Zhang, B.; Lin, Y.; Wang, Q.; Zhang, Q.; Su, D. S. Enhanced Chemoselective Hydrogenation through Tuning the Interaction between Pt Nanoparticles and Carbon Supports: Insights from Identical Location Transmission Electron Microscopy and X-Ray Photoelectron Spectroscopy. *ACS Catal.* **2016**, *6* (11), 7844−7854.
(50) Yamashita, T.; Hayes, P. Analysis of XPS Spectra of $Fe^{2+}$ and $Fe^{3+}$ Ions in Oxide Materials. *Appl. Surf. Sci.* **2008**, *254* (8), 2441−2449.
(51) Long, F.; Wu, S.; Chen, Y.; Cao, X.; Zhao, J.; Liu, P.; Jiang, J.; Zhang, X.; Xu, J. Hydrogenation of Fatty Acids to Fatty Alcohols over $Ni_3Fe$ Nanoparticles Anchored on $TiO_2$ Crystal Catalyst: Metal Support Interaction and Mechanism Investigation. *Chem. Eng. J.* **2023**, *464*, No. 142773.
(52) Zhang, W.; Lu, G.; Cui, C.; Liu, Y.; Li, S.; Yan, W.; Xing, C.; Chi, Y. R.; Yang, Y.; Huo, F. A Family of Metal-Organic Frameworks Exhibiting Size-Selective Catalysis with Encapsulated Noble-Metal Nanoparticles. *Adv. Mater.* **2014**, *26* (24), 4056−4060.
(53) Zhao, H.; Li, B.; Zhao, H.; Li, J.; Kou, J.; Zhu, H.; Liu, B.; Li, Z.; Sun, X.; Dong, Z. Construction of a Sandwich-like UiO-66-$NH_2$@Pt@m$SiO_2$ Catalyst for One-Pot Cascade Reductive Amination of Nitrobenzene with Benzaldehyde. *J. Colloid Interface Sci.* **2022**, *606*, 1524−1533.
(54) Zhuang, S.; Cheng, R.; Wang, J. Adsorption of Diclofenac from Aqueous Solution Using UiO-66-Type Metal-Organic Frameworks. *Chem. Eng. J.* **2019**, *359*, 354−362.
(55) Zhu, J.; Chen, H.; Wang, L.; Fu, E.; Wu, J.; Zhang, Q.; Yang, L.; Xu, G. High-Efficient Dynamic Kinetic Resolution of Amines with a Core-Shell Hollow Mesoporous MIL-101@Pd@ZIF-8 Nanocatalyst and Lipase. *Microporous Mesoporous Mater.* **2022**, *329*, No. 111490.
(56) Yu, D.; Duan, C.; Gu, B. UiO-66-$NH_2$@$MnFe_2O_4$ as a Novel and Retrievable MOF Nanocatalyst for Biodiesel Synthesis from Utilized Edible Oil in a Microwave Reactor: RSM Design and CI Engine Studies. *Renew. Energy* **2023**, *219*, No. 119338.
(57) Zhang, K.; Xi, Z.; Wu, Z.; Lu, G.; Huang, X. Visible-Light-Induced Selective Oxidation of Amines into Imines over UiO-66-$NH_2$@Au@COF Core−Shell Photocatalysts. *ACS Sustain. Chem. Eng.* **2021**, *9* (37), 12623−12633.
(58) Liu, X.; Yang, M.; Deng, Z.; Dasgupta, A.; Guo, Y. Hydrothermal Hydrodeoxygenation of Palmitic Acid over Pt/C Catalyst: Mechanism and Kinetic Modeling. *Chem. Eng. J.* **2021**, *407*, No. 126332.
(59) Fogler, H. S. *Elements of Chemical Reaction Engineering*; Ghosh, A. K.; Prentice-Hall of India Private Limited, 2004.
(60) Miyabe, K.; Isogai, R. Estimation of Molecular Diffusivity in Liquid Phase Systems by the Wilke−Chang Equation. *J. Chromatogr. A* **2011**, *1218* (38), 6639−6645.
(61) Seader, J. D.; Henley, E. J.; Roper, D. K. *Separation Process Principles: Chemical and Biochemical Operations*, Third ed.; John Wiley & Sons: Chichester, 2011.
(62) Arora, P.; Grennfelt, E. L.; Olsson, L.; Creaser, D. Kinetic Study of Hydrodeoxygenation of Stearic Acid as Model Compound for Renewable Oils. *Chem. Eng. J.* **2019**, *364*, 376−389.
(63) Sun, Y.; Ma, Q.; Ge, Q.; Sun, J. Tunable Synthesis of Ethanol or Methyl Acetate via Dimethyl Oxalate Hydrogenation on Confined Iron Catalysts. *ACS Catal.* **2021**, *11* (8), 4908−4919.
(64) Yue, S.; Ding, X.; Liu, X.; Guo, Y.; Wang, Y. High-Efficient Production of Fatty Alcohol via Hydrogenation of Fatty Acid over Cu-NbOx/SBA-15 Catalyst. *Catal. Today* **2022**, *405−406*, 221−226.
(65) Liu, K.; Pritchard, J.; Lu, L.; Putten, R. van; Verhoeven, M. W. G. M.; Schmitkamp, M.; Huang, X.; Lefort, L.; Kiely, C. J.; Hensen, E. J. M.; Pidko, E. A. Supported Nickel−Rhenium Catalysts for Selective Hydrogenation of Methyl Esters to Alcohols. *Chem. Commun.* **2017**, *53* (70), 9761−9764.
(66) Shi, D.; Vohs, J. M. Deoxygenation of Biomass-Derived Oxygenates: Reaction of Furfural on Zn-Modified Pt(111). *ACS Catal.* **2015**, *5* (4), 2177−2183.
(67) Morgan, K.; Goguet, A.; Hardacre, C. Metal Redispersion Strategies for Recycling of Supported Metal Catalysts: A Perspective. *ACS Catal.* **2015**, *5* (6), 3430−3445.